CERN/EF/RF 82-9
5 November 1982

RESULTS OF THE TEST OF THE SINGLE CELL 500 MHz ACCELERATING CAVITIES FOR THE PETRA FIVE-CELL CAVITY

Ph. Bernard, D. Bloess, G. Cavallari, E. Chiaveri, E. Haebel,
H. Lengeler, P. Marchand, J. Tückmantel and W. Weingarten

CERN, Geneva, Switzerland

H. Piel

University of Wuppertal, West Germany

ABSTRACT

In a series of measurements of four single-cell 500 MHz accelerating cavities assembled from two half cells and one intermediate ring fields higher than 6 MV/m (maximum 7.9 MV/m at 2.5 K) were consecutively reached at the first cooldown by local surface improvement before the cold test.

EF/0916G/WW/sf

1. INTRODUCTION

At CERN a five cell 500 MHz superconducting accelerating cavity is under construction. It is foreseen to be installed in the PETRA Storage Ring in 1983. It will be equipped with the necessary r.f. ports for the input of the power needed for the acceleration of the beam and for the output of the power deposited in the cavity by the bunch (fig. 1).

In the first stage of the production process the five cells are fabricated and tested individually. After all of them have shown satisfactory performance, their beam tubes are cut and the five individual cells are welded together at the iris openings. This work is currently under way at CERN.

In this report we want to describe the fabrication method for the individual cells and give the results of the individual tests.

2. FABRICATION

As the equatorial holes for the different couplers present a problem for the welding, we adopted a method, by which the crossing of welding seams is avoided. Apart from one cavity, which was fabricated in the traditional way with an equatorial welding, the individual cells are assembled together from three parts, an equatorial ring, which bears the coupler and antenna holes, and two half shells, which contain the beam holes (fig. 2).

The fabrication procedure is as follows: the ring is shaped by hydroforming, the half shells by spinning on a lathe from 2 mm thick niobium sheet material. These three parts are chemically polished by 70 μm and covered with an oxide layer by anodization (100 V) for detecting surface inclusions. Their final assembly is done by electron beam welding. Thereafter, the coupler and antenna holes are extruded and the coupler and antenna ports welded to the cell. The welds and the surface are carefully inspected by an optical telescope and, if necessary, imperfections at the weld like protrusions and welding beads or local surface contaminations are removed by grinding with an emery paper abrasive tool. Subsequently, we apply what we call our <u>standard treatment</u> i.e., degreasing, chemically polishing (20 μm), $H_2O + H_2O_2$ rinsing under ultrasonic agitation, and optical inspection (final control). If imperfections at the weld or contaminations are still detected, the standard treatment is started once again. If not, the cavity is rinsed in dust free and distilled water, dried in a horizontal position under dust free laminar air flow and mounted to the vacuum system.

The test of the cavity is performed in a horizontal position by which the electron loading is reduced significantly compared to a set-up with the cavity in a vertical position [1]. Control of the mechanical tolerances for this fabrication procedure gave the following result: absolute deviation of diameters from design value -0.3 mm, reproductibility of diameters ± 0.15 mm and length reduction (welding shrinkage plus deformation) due to welding at the iris 1.2 mm/weld.

3. EXPERIMENTAL RESULTS AND DISCUSSION

We had decided to do measurements on the single cell cavities instead of performing them on the complete 5-cell structure because we wanted to be able to apply temperature mapping diagnostics by means of available equipment. The main goal of the measurements at liquid helium temperature (table 1) was to find out the Q-value, the maximum field, and the mechanism and location of field breakdown. Had one cavity shown an unsufficient accelerating field, we would have applied local mechanical methods for increasing the field [1]. One remarkable outcome of this test series, however, was that we were able to reach satisfactory accelerating fields at the first cold test.

Measurements at room temperature (table 2) were performed to determine the external Q of the various couplers and for the different modes, which is crucial to determine the power to be additionally dissipated in the cavity by the passage of the bunch, and to estimate the maximum current to be allowed. In addition we measured, how the mode frequencies are changed by varying the length of a cell, which will be used for the fine tuning of the five cell cavity to the PETRA frequency.

3.1 Electron loading

Although no electron loading was observed in a test of a single cell cavity of similar shape equipped with only the main coupler port [1], we were aware that local field configurations at the r.f. probe and coupler ports might favour electron multipacting.

Indeed, all cavities exhibit strong electron loading at the start of the experiment (associated with microamperes of current picked up by a probe in the beam tube). This is reduced to an unsignificant level by "r.f. processing" within some hours. This kind of electron loading was observed at distinct field levels (1.4, 2.5, 3.0, 4.5 MV/m) which were within experimental errors the same for the different cavities tested. This is a clear indication for resonant electron loading (multipacting). These field levels showed up in field limitations (no increase of field possible by an increase of the power available) and in field breakdowns (quenches). The quench location was mostly found at the location of the magnetic field enhancement at the higher order mode coupler hole (occasionally at the main coupler hole). These quenches were associated by a burst of electrons picked up by the electron probe. At least for two cavities (1,5) an enhancement of this current was still detected after high field operation at the level 4.5 MV/m (fig. 3), without a quench being observed. This is in agreement with measurements in other laboratories [2]. Attempts to overcome the thresholds faster by r.f. helium ion sputtering were not successful. Once, we observed such a field threshold at a low field to reappear after the operation of the cavity at high field.

All this information put together lead us to the conclusion, that this resonant electron loading is very probably located at the higher order mode coupling port. It does not harm the cavity performance. The quenches observed during the first field increase were induced by resonant electron loading.

In addition we also observed non resonant electron loading. In test No. 1 it was possible to increase the breakdown field level from 5.5 MV/m to 7.3 MV/m by helium ion sputtering of some hours, which is an effective countermeasure against non resonant electron loading. During the sputtering the electron current picked up decreased. Pumping off the helium gas did not change the good performance of the cavity.

In test No. 4 the quench location was found to be located on a line like loss region due to electron impact. From these observations we conclude that we have also observed quenches due to non-resonant electron loading.

We would like to state, that in no case we observed a large reduction in Q-value due to electron loading (fig. 5).

3.2 Losses at weldings

We could confirm that even at the highest fields losses at welds are not visible by temperature mapping diagnostics (fig. 4) [1].

3.3 Overall losses

For the sake of an easy and fast experiment we had equipped the cavities with short beam tubes which we knew would limit the Q-value due to losses in the beam tube cover and joint. Thus the Q-value would not inform on the overall surface losses. This made us determine them from the temperature maps.

The temperature maps confirmed that the surface losses are dominated by frozen in magnetic flux [1]. In fig. 6 the local surface resistance R_s at 7 MV/m is plotted, which was determined by the relation $R_s = 2\,\dot{Q}/H^2$. $\dot{Q}$ is the local heat current measured by the temperature mapping system at 2.9 K [3], H is the local magnetic field. Fig. 6(a) shows R_s, averaged over the azimuth, as a function of the latitude s. The strong enhancement of losses near the equator, where the frozen in magnetic flux is dominant, is clearly visible. In fig. 6(b) R_s is plotted for constant latitude in the region of maximum magnetic field as a function of the azimuth.

The ambient magnetic field in the cryostat was determined to 130 mOe(*) parallel to the vertical cryostat axis. If the surface resistance R_s is mainly due to frozen in magnetic flux, it should follow a relation $R_s \sim R_1\ |\cos\phi|$, which is indicated in the figure. R1 amounts to 500 nΩ.

(*) If it is assumed, that the magnetic flux is not expelled, a magnetic field of 130 mOe corresponds to 6.5 x 10^5 flux lines per cm^2. Assuming 550 Å for the coherence length of niobium, this is equivalent to a normal conducting area of 6 x 10^{-5} cm^2. A typical surface resistance for normal conducting niobium at 10 K and 500 MHz is 3 mΩ, which yields 200 nΩ average surface resistance.

Losses of different origins contribute by 30 nΩ, from which we conclude that $Q \approx 10^{10}$ at 2.9 K would have been attained by carefully shielding the ambient magnetic field.

4. CONCLUSION

In a series of measurements on four single cell cavities (with intermediate ring) we surpassed an accelerating field of 6 MV/m at the first test. We consider this to be the most important issue of this test series. This gives us the feeling of a safety margin big enough to reach 3 MV/m, which is foreseen for the PETRA test. In our opinion, the whole sequence and careful control of fabrication and treatment steps is responsible for this achievement: the careful optical inspection of half shells, the local mechanical treatment thereafter, the optical inspection of the fully assembled cavity including weldings, and the local mechanical treatment and chemical polishing. All the other equally important features of the standard treatment are described elsewhere [1].

From the success of the test series described in this paper we conclude that we have been able to eliminate lossy spots before the test. We were no longer obliged to remove the lossy spots after the test, as described in [1]. This gives us hope that the fabrication of a 5-cell cavity which fulfills the design values from the beginning is feasible.

Acknowledgements

We would like to thank our technicians for their help. This work had to rely strongly on the skill and competence of the SB workshop for spinning, electron beam welding, brazing and chemical treatments. We also thank the EF workshop and cryogenic group for their help.

REFERENCES

[1] Ph. Bernard et al., CERN/EF 82-8 (1982) (to be published in Nucl. Instr. & Meth.).

[2] K. Yoshida et al., IEEE Trans. Nucl. Sci. NS-26 (1979) 4114.

[3] R. Romijn and W. Weingarten, CERN/EF/RF 81-4, Int. Note (1981).

TABLE 1

Results of tests of single cells for the PETRA cavity

Cell No.	Inter-mediate ring	f_0 (MHz) [f_{eff} (4.2 K)(a)]	Treatment & operation conditions	Q_0(b) (10^9) low field	High(b) field	E_{acc} (MV/m) Start of electron loading(c)	E_{max} (4.2 K)	E_{max} T < 4.2 K	Quench location
1	yes	498.726 |500.03|	Standard(d) He ion sputtering	1.2	0.8	5.0	7.3	7.6	Near iris
2	no	497.403 |499.90|	Standard r.f. processing	1.4	1.3	None	5.0	-	Field enhancement region of main coupling port
3	yes	496.777 |499.28|	Stand. r.f. processing (leak)	1.1	-	None	6.8	-	Weld in high magnetic field region
4	yes	497.499 |500.0|	Standard r.f. processing	1.0	0.8	4.0	6.4	-	Near iris (at electron trajectory)
5	yes	498.728 |500.03|	Standard He ion sputtering	1.1	0.9	5.6	7.6	7.9	Field enhancement of HOM coupling port

(a) f(π-mode, 5-cell) = f(1-cell) + 2.53 MHz; f(PETRA) = 499.665 MHz.

(b) Limited by beam tube cover and joint losses.

(c) $I_e > 1$ pA; I_e is the electron current picked up at the beam hole.

(d) Inspection and grinding of half cells, CP 70 μm; inspection and grinding of welds, CP 20 μm; rinsing with dust free distilled water, horizontal position.

<u>TABLE 2</u>

Radio-frequency measurements (room temperature in air)

Mode	Accelerating	TM011	TM110	TM0111	TM021	TM012
f[MHz] (1)	498.258	920.48	733.93, 734.43	1049.59, 1050.08	1373.64	1468.59
(2)	497.08	-	-	-	-	-
(3)	496.3	912.28	731.46, 731.88	1042.55, 1042.80	1366.10	1454.61
(4)	497.1	-	-	-	-	-
(5)	498.253	920.79	733.67, 734.33	1049.25, 1049.70	1373.03	1468.72
Q_{ext} (HOM-loop coupler)	-	-	15 000	-	-	3×10^5
Q_{ext} (HOM-antenna-coupler)	-	8400	-	5200	6000	-
Q_{ext} (antenna probe)	$> 2 \times 10^{10}$	2×10^9	$> 2 \times 10^{10}$	$> 6 \times 10^8$	$> 5 \times 10^8$	2×10^8
$\Delta f/\Delta l$ [kHz/mm]	380	110	110	455	- 910	- 575

<u>N.B.</u> f = frequency; Q_{ext} = external Q; $\Delta f/\Delta l$ = frequency change per unit length change; $\Delta f/\Delta p$ = frequency change per unit pressure change; $\Delta f/\Delta p \approx -200$ Hz/mbar
f(4.2 K) - f(300 K) = 460 kHz.

FIGURE CAPTIONS

Fig. 1 5 cell superconducting accelerating cavity to be installed in the PETRA Storage Ring.

Fig. 2 An individual cell is fabricated out of two half shells and an equatorial ring. In the upper photo two ground regions are visible.

Fig. 3 Enhancement of electron current at 4.5 MV/m picked up by a probe in the beam hole. The line may guide the eye.

Fig. 4 Temperature map at 7.3 MV/m. There is no enhancement of losses visible at the weld (arrows).

Fig. 5 The field dependence of the Q-value. Q-values are dominated by the losses of the beam tube end cover and joint.

Fig. 6 (a) Average surface resistance as a function of the latitude s.

(b) Surface resistance as a function of the azimuth near cavity equator. The curves correspond to the ambient magnetic field perpendicular to the cavity axis assumed to be totally frozen into the surface.

for test at PETRA

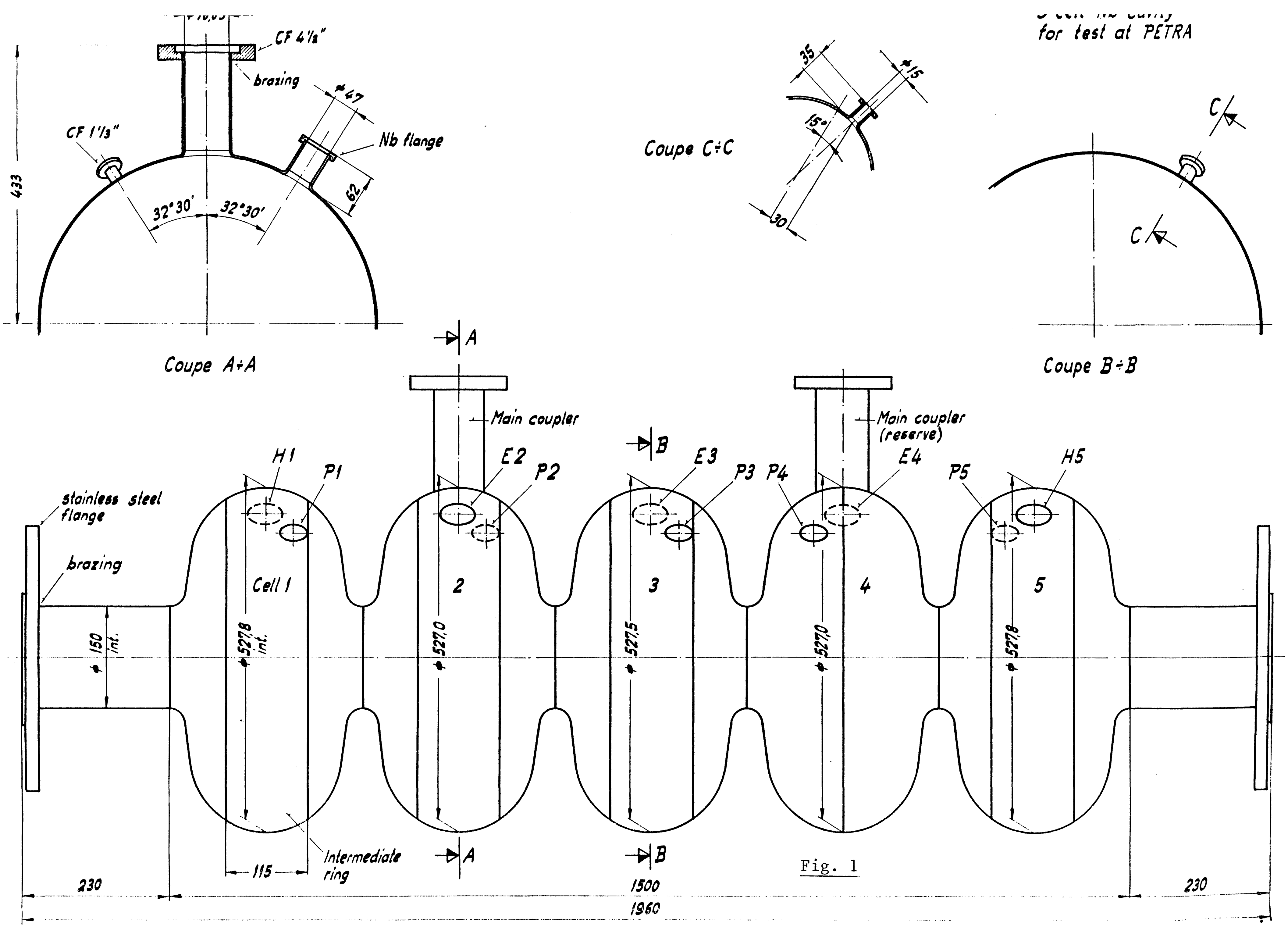

Fig. 1

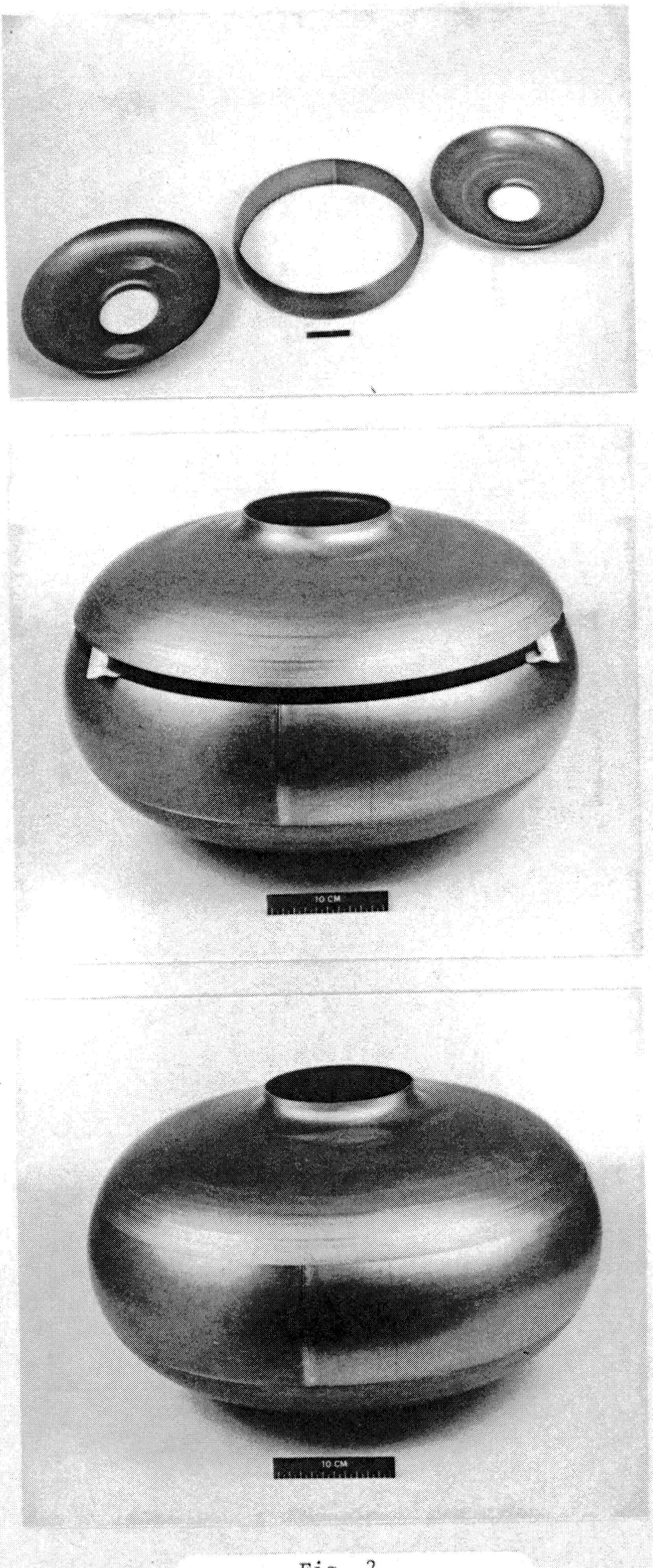

Fig. 2

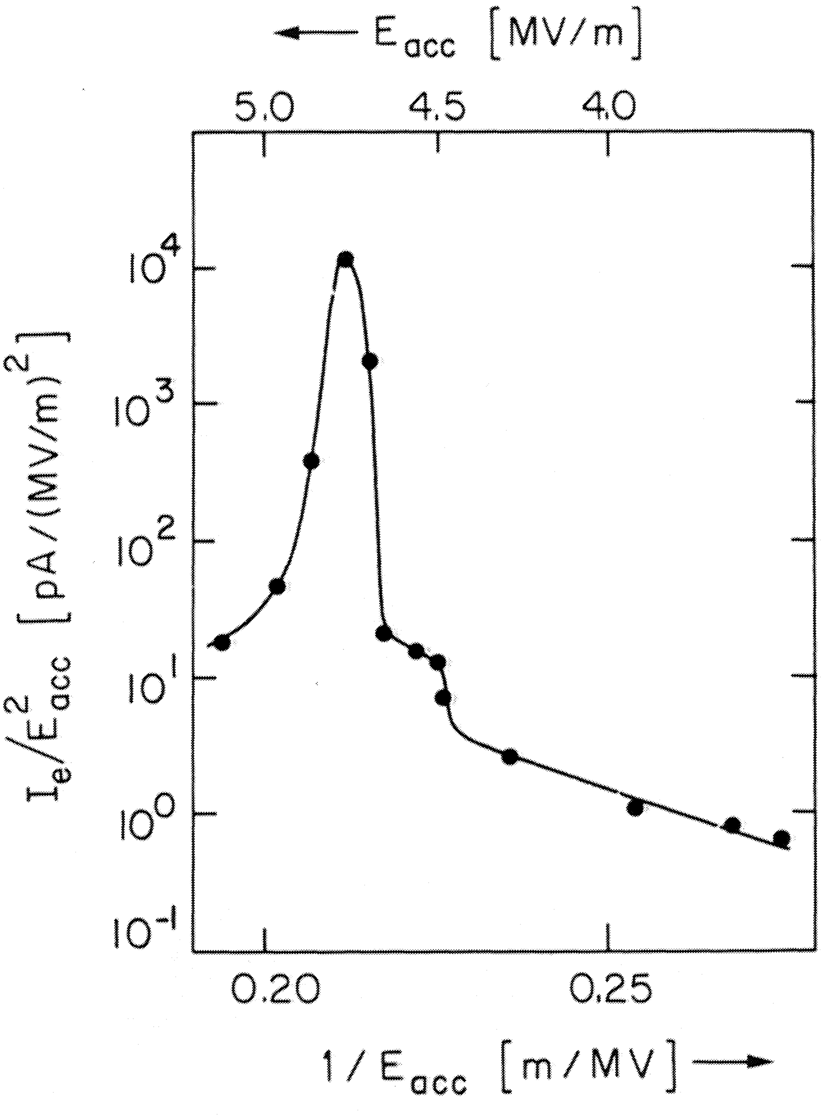

← E_{acc} [MV/m]
5.0
4.5
4.0
10^4
10^3
10^2
10^1
10^0
10^{-1}
I_e/E_{acc}^2 [pA/(MV/m)^2]
0.20
0.25
$1/E_{acc}$ [m/MV] →

Fig. 3

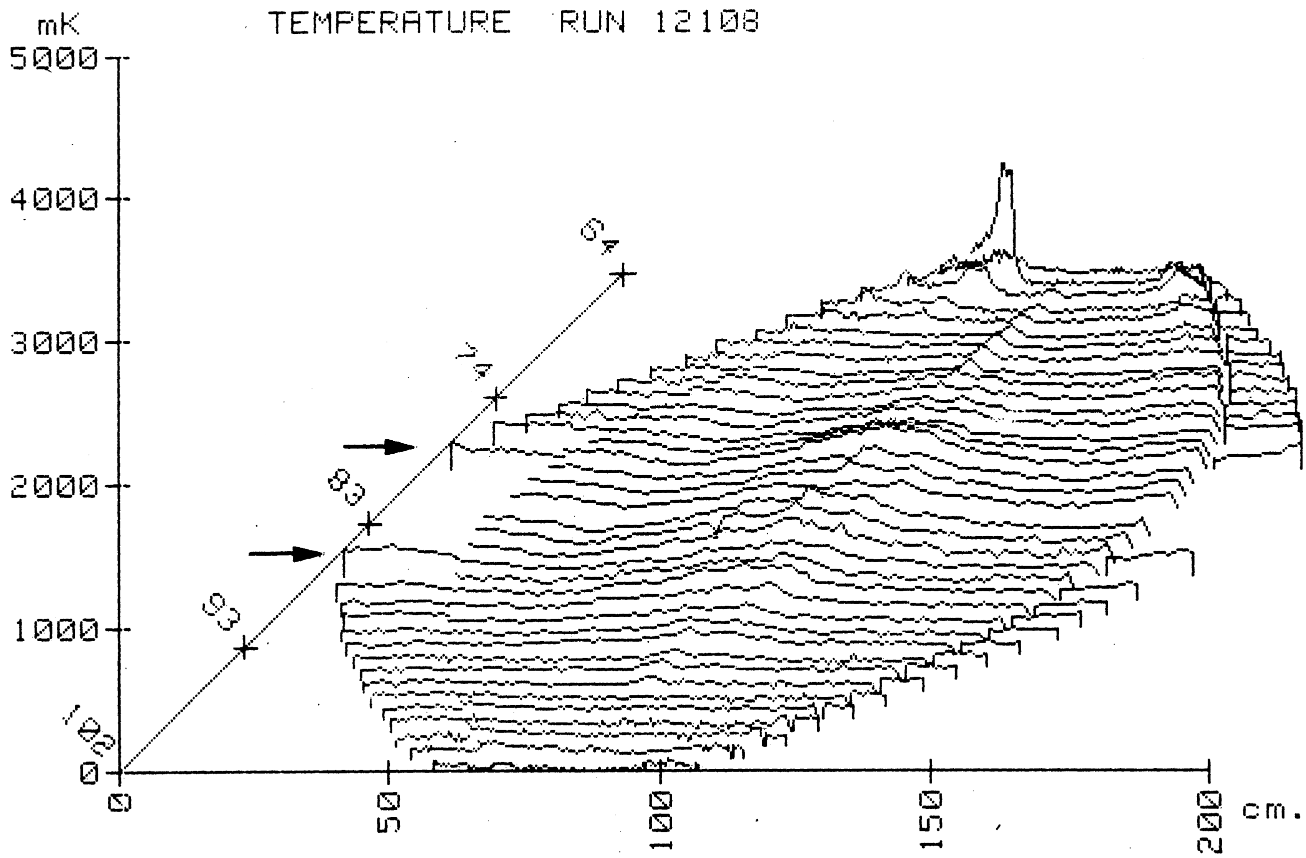

mK
TEMPERATURE RUN 12108
5000
4000
3000
2000
1000
0
64
74
83
93
102
0
50
100
150
200
cm.

Fig. 4

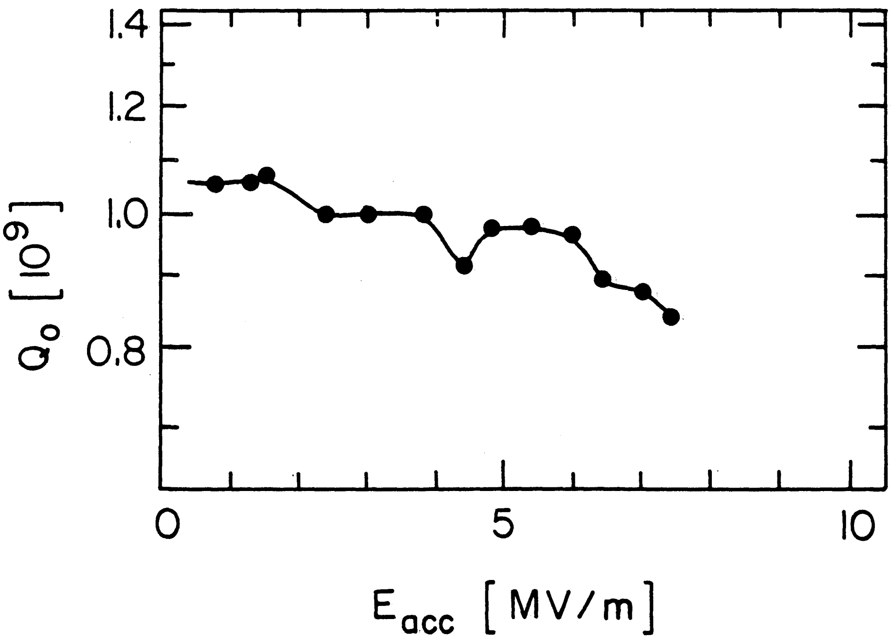

Fig. 5

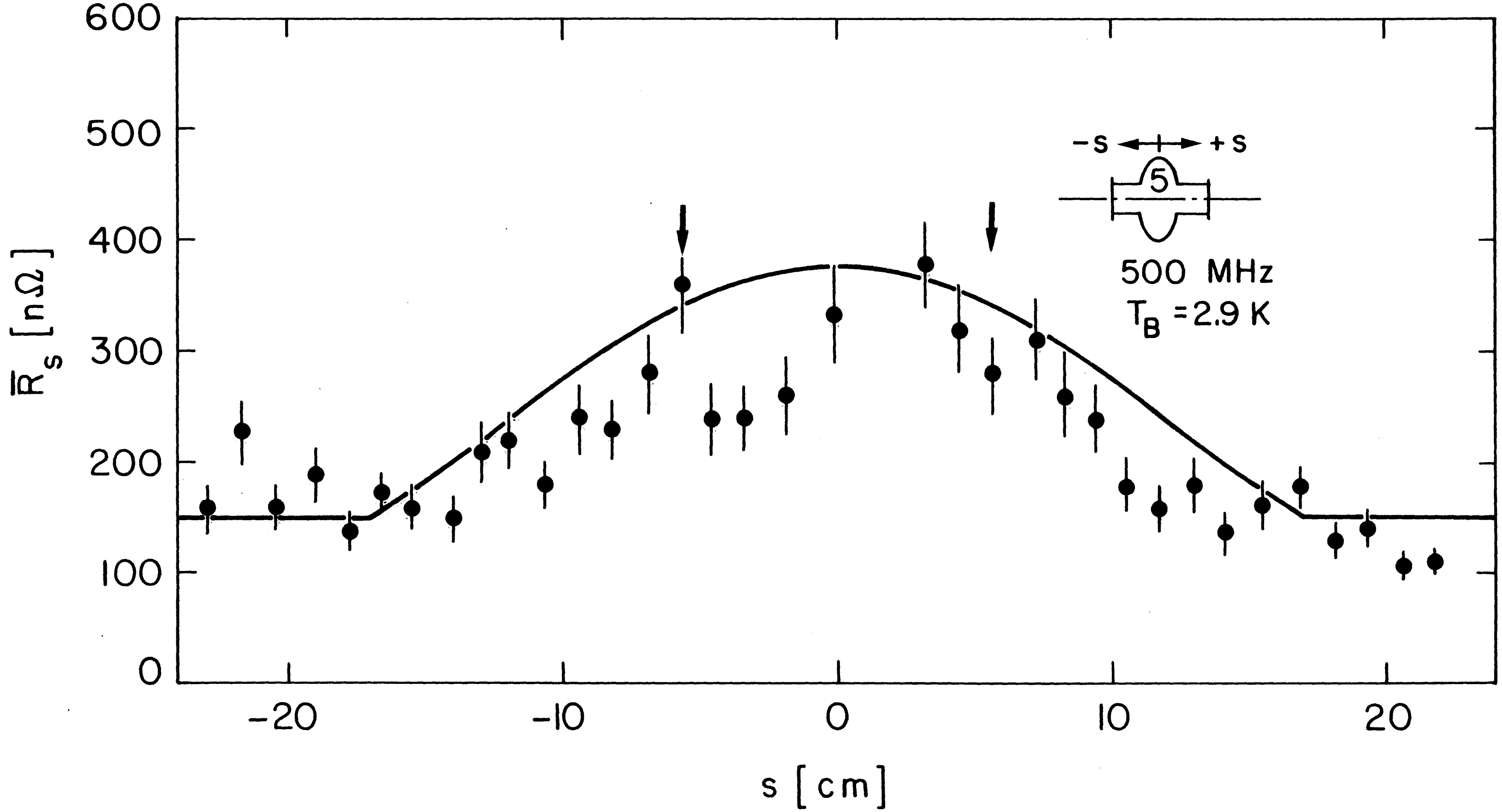

Fig. 6(a)

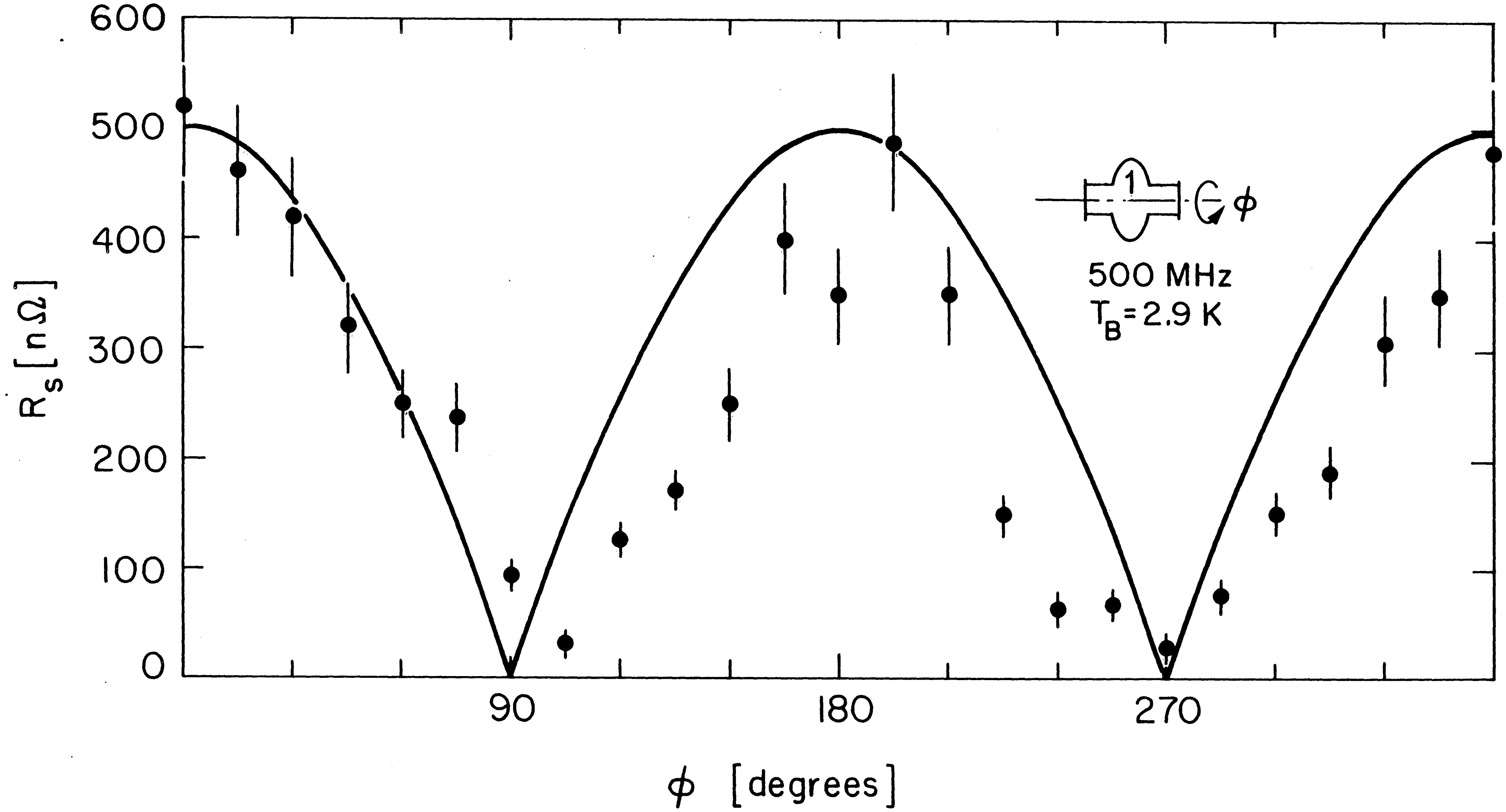

600
500
400
300
200
100
0
R_s [nΩ]
90
180
270
φ [degrees]
1
φ
500 MHz
T_B=2.9 K

Fig. 6(b)